Cluster crystals with combined soft- and hard-core repulsive interactions

Lorenzo Caprini,[1] Emilio Hernández-García,[2] and Cristóbal López[2]
[1]*Gran Sasso Science Institute (GSSI), Via F. Crispi 7, 67100 L'Aquila, Italy*
[2]*IFISC (CSIC-UIB), Instituto de Física Interdisciplinar y Sistemas Complejos, Campus Universitat de les Illes Balears, E-07122 Palma de Mallorca, Spain*

(Received 18 July 2018; published 19 November 2018)

Particle systems interacting with a soft repulsion, at thermal equilibrium and under some circumstances, are known to form cluster crystals, i.e., periodic arrangements of particle aggregates. We study here how these states are modified by the presence of an additional hard-core repulsion, accounting for particle size. To this end we consider a two-dimensional system of Brownian particles interacting through a potential which includes hard-core and soft-core (of the GEM-α type) repulsive terms. The system shows different phases, and we focus in the regime where cluster crystals form. We consider two situations: the low-temperature one in which particles inside the clusters also show an ordered structure (crystal cluster-crystal phase), and the one occurring at higher temperature in which particles within the clusters are spatially disordered (fluid cluster crystal). An explicit expression for the energy in terms of the typical distance between clusters and the typical distance of the particles within the clusters is obtained for vanishing temperature, from which mean mean inter- and intracluster distances are obtained. Finite-temperature corrections are also discussed, considering explicitly the role of entropy.

DOI: 10.1103/PhysRevE.98.052607

I. INTRODUCTION

Particles interacting via soft-core repelling forces may crystallize in equilibrium into ordered structures, with a unit cell composed of a closely packed cluster of particles [1–7]. This is a particularly relevant situation for some polymers, dendrimers, or colloidal solutions, where the effective potentials between their centers of mass are soft and repulsive [4,8,9]. This phase, called cluster crystal, occurs for low temperatures and large enough density and packing fraction.

This type of system has been studied by using a variety of methods, from Monte Carlo to density functional theory [4,5], or in the related Dean-Kawasaki equation approach [10]. A mathematical criterion needed for the formation of cluster crystals is that the Fourier transform of the interparticle potential $\tilde{V}(k)$ should take negative values for some values of k [4,5,10]. For the commonly studied generalized exponential model (GEM-α), $V(r) = \epsilon \exp[-(r/R)^\alpha]$—which is an example of soft potential [8]—with ϵ an energy scale and R the typical interaction range, this happens when $\alpha > 2$. The occurrence of cluster crystals in GEM-α potentials with $\alpha > 2$ is related to the fact that as α increases the potential becomes more boxlike shaped. The physical mechanism leading to the cluster crystals is the balance between the repulsive forces among particles inside a cluster and the forces from neighboring ones [10].

The natural extension of considering a hard-core contribution into the potential, taking into account the finite size and impenetrable character of a core part of the interacting particles, was considered in [11]. A problem to study this type of system within a continuous-density description is that this approach leads to the consideration of the Fourier transform of the potential, which is in general not well defined in the hard-core case. The authors of [11] use instead a lattice model where the lattice constant equals the particle size and the hard-core repulsion is implemented by imposing single occupancy per site. Thus they generalize the soft-potential criterion for the appearance of cluster crystals to include terms depending on the occupied volume fraction. However, this lattice model cannot distinguish ordered from disordered states within the clusters. To avoid this the authors of Ref. [11] also introduced an off-lattice model with a particular type of potential known as hard-core soft-shoulder potentials. Further studies with the same potentials are found in [12,13] where, in particular, finite-temperature corrections and detailed phase diagrams are presented.

In this work, we focus on the study of two-dimensional off-lattice systems with repulsive interaction potentials related to the well-studied hard-core soft-shoulder case but more general than it. Specifically, we consider a soft repulsion of the GEM-α type at large distances, complemented by a strongly repulsive core behaving as r^{-b} at short distances. We keep the name of "hard core" for this part of the potential, although it is not strictly impenetrable. Under suitable parameters, in particular at low temperature, cluster-crystal phases are found. Our main question is to understand how the hard-core power-law potential changes the equilibrium configurations of particles interacting through the GEM-α potential. To understand the structures found, we compute the energy of the system by considering both the interactions between clusters and the interactions among particles within clusters. For this last contribution, at variance with previous studies [11–13], we explicitly take into account the intra-aggregate structure, i.e., whether the particles may order periodically or not inside every cluster. Mean inter- and intracluster distances are then obtained from energy minimization. We validate our results with numerical simulations of an ensemble of interacting Brownian particles in a thermal bath. Temperature corrections are also considered to estimate the typical cluster size, which is different at very low temperature, when the within-cluster

distribution of the particles shows an ordered structure with respect to higher temperatures, when the clusters are in a fluid or gas state.

The paper is organized as follows. In Sec. II we introduce the model, discuss the role of the spatial scales in the potential, and present the system's phases that will be studied. In Sec. III we derive an analytical expression for the energy of the system in the crystal crystal-cluster phase in the limit of small temperatures. In the subsequent Sec. IV we compute some temperature effects on cluster characteristics. We conclude with a summary and discussion in Sec. V.

II. MODEL AND CLUSTER-CRYSTAL PHASES

As one of the ways to obtain thermal equilibrium configurations under the type of interactions described above, we consider a d-dimensional system of N interacting Brownian particles of unit masses in contact with a thermal bath. We restrict our scope to a regime of very large friction, which allows us to neglect the inertial terms and to assume directly an overdamped dynamics:

$$\dot{\mathbf{x}}_i = -\nabla_i V(\mathbf{x}_1, \ldots, \mathbf{x}_N) + \sqrt{2D}\,\boldsymbol{\eta}_i, \quad i = 1, .., N, \quad (1)$$

where the noise vector $\boldsymbol{\eta}$ with component η_l verifies $\langle \eta_l \rangle = 0$ and $\langle \eta_l(t)\eta_m(t')\rangle = \delta(t-t')\delta_{l,m}$, with $l, m = 1, \ldots, d$. The diffusion coefficient D is proportional to the temperature through the Einstein relation $D = k_B T$ when time is measured in units of the inverse friction coefficient. The potential V is pairwise and contains two parts, a hard-core repulsion referring to the particle size V_h and a soft-core repulsive part V_s (they act at different scales as detailed later):

$$V(\mathbf{x}_1, \ldots, \mathbf{x}_N) = \sum_{1 \leqslant i < j \leqslant N} [V_h(|\mathbf{x}_i - \mathbf{x}_j|) + V_s(|\mathbf{x}_i - \mathbf{x}_j|)]. \quad (2)$$

We restrict to $d = 2$ and study all along this paper the particular cases of $V_h(r) = \epsilon_h(\frac{r_0}{r})^b$ and $V_s(r) = \epsilon_s \exp[-(r/R)^\alpha]$, with $r = |\mathbf{x}|$. V_s is the GEM-α potential, which accounts for an effective soft repulsive interaction with a typical length scale R and energy scale ϵ_s. V_h, modeling a hard core, is a standard power-law repulsion where r_0 stands for the typical length scale for the size of the particles. ϵ_h is an energy scale which can be absorbed in the definition of r_0, since it always appears in the combination $\epsilon_h r_0^b$. However, we keep this parameter explicit through the paper, as it helps to identify the terms in our expressions coming form the hard core. In the numerics it will be fixed as $\epsilon_h = \epsilon_s$. Despite the particular choice of potentials, we point out the generality of the arguments presented below.

In the absence of the hard-core potential the behavior of the system is well understood: for $\alpha > 2$, a small enough temperature, large enough numerical density, $\rho_0 = N/L^d$, and large packing fraction, $\phi = \rho_0 R^d$, cluster crystals are formed in which (point) particles aggregate in clusters separated by a distance proportional to R, with particles randomly moving inside each cluster [10]. Unveiling the effects of the hard-core potential on this phase is the main purpose in what follows. Note the difference with other studies considering cluster phases with short-range attraction and long-range repulsion [14–16]. In our setting, there is no attraction at any scale.

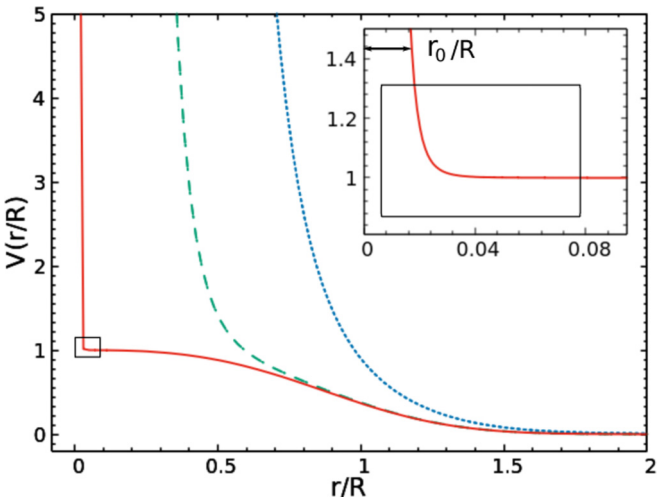

FIG. 1. Potential given by $V_s(r) + V_h(x)$ with $V_s(r) = \epsilon_s \exp[-(r/R)^3]$ and $V_h(r) = \epsilon_h(r_0/r)^6$. Fixing $R = 0.1$ and $\epsilon_h = \epsilon_s = 1$, the different lines correspond to $r_0 = 0.001$ (red solid line), 0.04 (green dashed line), and 0.1 (blue dotted line). In the inset, a zoom of the potential in the first case.

The shape of the total potential $V = V_h + V_s$ is shown in Fig. 1 for the special case $\alpha = 3$ and $b = 6$. If there is no scale separation, $r_0 \gtrsim R$ (green-dashed and blue-dotted lines in Fig. 1), the potential behaves effectively as just a hard-core repulsive one, since all of the features of the soft-core part are masked. This is qualitatively similar to setting $V_s = 0$. In this case, particles freeze at low temperatures, forming a hexagonal lattice. We will not discuss here the subtleties associated with the nature of this type of two-dimensional crystallization (see, for example, Ref. [17]). The interesting regime, assumed in the rest of the paper, occurs when $r_0 \ll R$ (red solid line in Fig. 1): the potential has an abrupt decrease up to the scale r_0, followed by a smoother one, as shown in the figure inset.

A. Cluster-crystal phases

As shown in Fig. 2, numerical simulations in a two-dimensional square box of size L with periodic boundary conditions show a phenomenology consistent with [11]. In particular, for $\alpha = 3$, $b = 6$ and restricting to densities and packing fractions large enough, cluster-crystal phases are found: at low enough temperature, particles aggregate in clusters which arrange hexagonally. Moreover, the average population of each cluster N_c increases with ϕ. The intercluster distance $\bar{x}$ is relatively insensitive to ϕ, increasing with just R. These are the usual properties of cluster crystals [4,5,10].

We discuss the effect of the temperature T, or equivalently, of the diffusion coefficient $D = k_B T$, by evaluating the microscopic structure of the system via the radial distribution function $g(r) = \rho_0^{-1}\langle \sum_{i \neq 0} \delta(\mathbf{x} - \mathbf{x}_i)\rangle$, where a target particle is at the origin, the sum is over the other particles, and the brackets indicate an equilibrium temporal (long-time) or thermal average, and also a circular average over positions $\mathbf{x}$ with the same modulus $|\mathbf{x}| = r$.

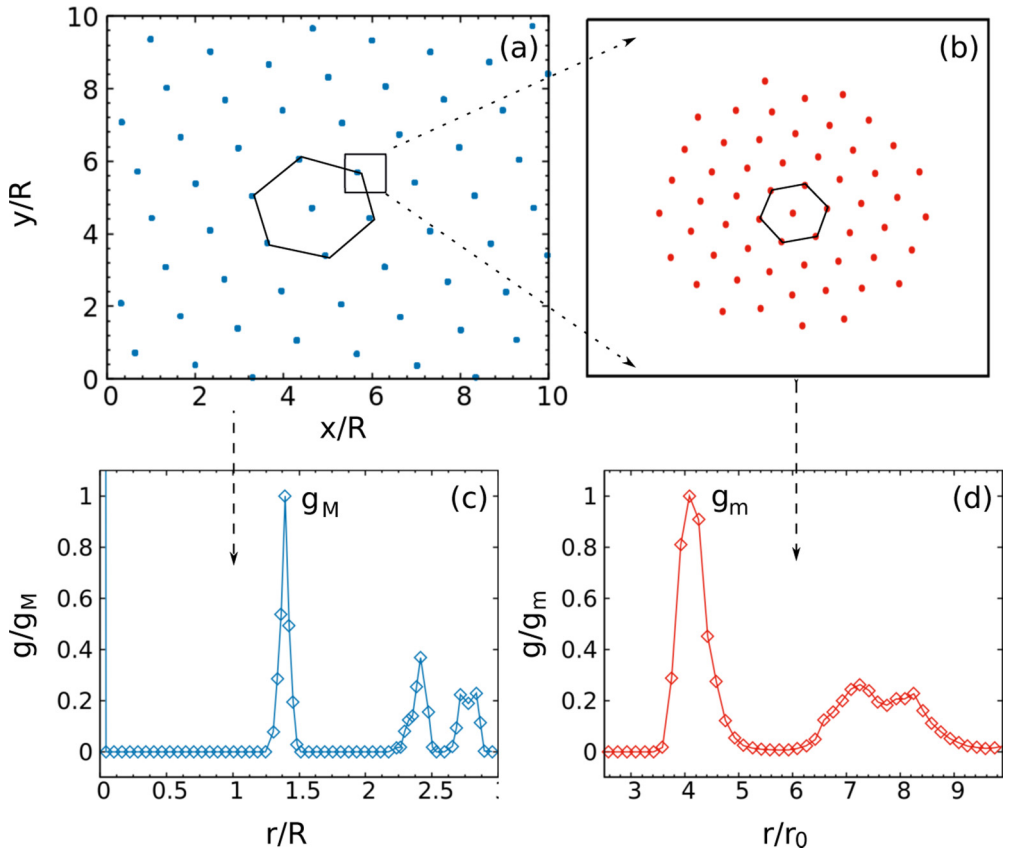

FIG. 2. Crystal cluster-crystal phase. Top panels: A snapshot of the system configuration in the x-y plane [panel (a)] and zoom into a single cluster [panel (b)]. Bottom panels: Radial correlation function $g(r)$ as a function of r/R [panel (c)]. This representation highlights the presence of a peak at $r \approx 1.4R$, indicating periodic ordering with this periodicity. Also visible is a huge peak at $r \approx 0$, indicative of particle clustering at small distances. A zoom of $g(r)$ on this peak is plotted in panel (d) as a function of r/r_0. This part of $g(r)$ characterizes the type of particle ordering inside the clusters. For presentation purposes, g is normalized by the height of the main peak in each graph. Parameters: $\alpha = 3$, $b = 6$, $L = 1$, $N = 1000$, $r_0 = 10^{-3}$, $R = 10^{-1}$, $\epsilon_s = \epsilon_h = 1$, $D = 10^{-6}$.

The comparison of $g(r)$ at small distances with typical radial distribution functions of a simple solid, liquid, or gas allows us to identify solid-, liquid-, and gaslike aggregation phases inside the clusters, which coexist with the cluster-crystal structure at much larger distances. Since the number of particles in the clusters is small, these states cannot be interpreted as real distinct macroscopic phases. For this reason, a rigorous discussion about phase transitions is meaningless and we restrict our considerations to the qualitative configuration of the system, for which the following observations are made:

(1) For small temperatures, particles inside each cluster are almost frozen, showing a hexagonal arrangement. This is the ordered crystal phase identified in [11], which is shown in the top row of Fig. 2. The left panel shows the crystal of clusters and the right one a zoom of one cluster, with the particles perfectly ordered. The lower row shows $g(r)$ at the scale of the clusters (left panel) and a zoom into the peak in the region $r \approx r_0$, displaying the crystalline ordering of the particles within clusters (right panel). From the position of the peaks in both figures, we can obtain the equilibrium distance among clusters $\bar{x}_e \approx 1.4R$ (left panel) or among particles $\hat{x}_e \approx 4.05r_0$ (right). As in a solid, particles fluctuate around their equilibrium positions, but these fluctuations are very small compared to $\hat{x}_e$. We observe that in the steady state, after a long time transient, the hexagonal clusters become aligned so that the lines joining their centers coincide with their apothems: the crystal is completely ordered.

(2) Upon increasing the temperature, particle positions disorganize and a liquidlike phase appears inside each cluster. As in a simple liquid, particles move around the whole cluster volume. In Fig. 3, $g(r)$ at the small scales is shown (green $D = 10^{-4}$ and yellow $D = 10^{-3}$ lines), revealing a crossover from solid to fluid characteristics.

(3) A further increase of T produces the growth of the cluster volume. Particles within each cluster form a gaslike phase, as revealed by the absence of well-defined secondary peaks in Fig. 3 (red $D = 10^{-2}$ line).

(4) Further increase of the diffusion coefficient or temperature makes the clusters disappear, leaving a global fluid phase. On the other hand, by increasing ϕ, we observe the lamellar and micelle phases described in [11]. However, as mentioned in the Introduction, we restrict our study to the range of temperatures or volume fractions where only the different types of cluster crystals appear.

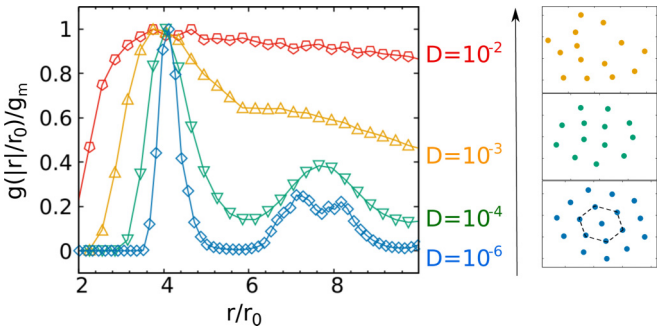

FIG. 3. $g(r)/g_m$ (g_m is the maximum value of g) at small scales $r \approx r_0 \ll R$ for different diffusion coefficients $D = k_B T = 10^{-6}, 10^{4}, 10^{-3}, 10^{-2}$, respectively corresponding to blue diamonds, green upper triangles, orange lower triangles, and red pentagons. On the right we show a snapshot of within-cluster particle distributions corresponding to each of the three lower temperatures. Remaining parameters: $\alpha = 3$, $b = 6$, $L = 1$, $N = 10^3$, $r_0 = 10^{-3}$, $R = 10^{-1}$, $\epsilon_s = \epsilon_h = 1$.

III. CLUSTER ENERGY

We now set up an energy calculation which is useful to understand the observed structures and phenomenology, in particular, the steady-state properties of the system: the distance between clusters, the lattice type, and the average size of the clusters. In this section we are restricted to very small T, i.e., to the crystal cluster-crystal phase, numerically discussed in the previous section. In this regime any entropic contribution does not significatively affect the free energy, as is expected in the solid state. In the next section we will consider finite-temperature corrections, and the role of the entropy will be explicitly taken into account. Note that, as mentioned in the Introduction, we avoid any description based on the coarse-grained density of particles. This is similar to the off-lattice approach followed by [11] for the hard-core soft-shoulder cases, but extended here to our more general class of potentials.

We rewrite the total energy into two contributions: a self-energy of the clusters themselves, E_C, and an interaction energy among them, E_I. Two main quantities are fundamental: the mean intercluster distance $\bar{x}$ and the mean interparticle distance inside a cluster $\hat{x}$. Indeed, the number of clusters in the system, n_c, can be estimated as $n_c = \chi L^d/\bar{x}^d$ (for arbitrary dimension d), where χ is a parameter which depends on the lattice, for instance, $\chi = 1$ for a square lattice and $\chi = 2/\sqrt{3}$ for a triangular one. If we denote as N_c the average number of particles of each cluster, then $N = n_c N_c$, so that we can write $N_c = \bar{x}^d \rho_0/\chi$. The average size of the cluster σ_c can be estimated from $\hat{x}$ and N_c, considering the hexagonal arrangement of the intracluster particles.

In the following we work in two dimensions, but our approach can be extended to three-dimensional systems. As mentioned, for small enough temperature we can neglect entropic contributions and the equilibrium properties are all determined by the total energy $E = E_C + E_I$, where

$$E_C = n_c \sum_{1 \leqslant i < k}^{N_c} [V_h(|\mathbf{x}_i - \mathbf{x}_k|) + V_s(|\mathbf{x}_i - \mathbf{x}_k|)]. \quad (3)$$

Since r_0 is very small and V_s decays fast with distance, it is a reasonable approximation for the intercluster energy to consider only interactions of particles in neighboring clusters, so that

$$E_I \approx n_c \frac{\gamma_I}{2} E_I^{a,b} = n_c \frac{\gamma_I}{2} \sum_{k_b, i_a = 1}^{N_c} \left[V_s\left(\left|\mathbf{x}_{i_a} - \mathbf{x}_{k_b}\right|\right) + V_h\left(\left|\mathbf{x}_{i_a} - \mathbf{x}_{k_b}\right|\right)\right], \quad (4)$$

where $E_I^{a,b}$ is the interaction energy between two neighboring clusters, which we denote by a and b, and $\mathbf{x}_{i_a}$ ($i_a = 1, \ldots, N_c$) is the position of the ith particle in the cluster a. The constant γ_I is the number of first neighbors in the lattice in which the clusters arrange (in two dimensions $\gamma_I = 6$ for a hexagonal lattice, or $\gamma_I = 4$ for a square lattice). Since we assume a separation of scales of both potential terms, we consider $\bar{x}$ and $\hat{x}$ independent variables and look for an expression for the energy such that $E = E(\bar{x}, \hat{x}) = E_I(\bar{x}, \hat{x}) + E_C(\bar{x}, \hat{x})$. As already mentioned, for T small enough, the equilibrium configuration is the one that minimizes the total energy with respect to $\bar{x}$ and $\hat{x}$. Let us point out that because of the relation between $\bar{x}$ and N_c, at constant density the minimization with respect to $\bar{x}$ is formally equivalent to that with respect to N_c, exploited within the density functional approach in previous works [18,19] for purely soft-core potentials.

To proceed we introduce the particular forms of V_h and V_s and make use of their properties. In the following we are labeling different clusters with letters $a, b, \ldots = 1, 2, \ldots, n_c$ and the particles with indices $i, j, \ldots = 1, \ldots, N$, or if we want to specify the ith particle of cluster a we use $i_a = 1, \ldots, N_c$. Let us first work out the self-interaction cluster energy:

$$\begin{aligned} E_C &= n_c \sum_{i<k}^{N_c} \left[\epsilon_s e^{-(|\mathbf{x}_i - \mathbf{x}_k|/R)^\alpha} + \epsilon_h \left(\frac{r_0}{|\mathbf{x}_i - \mathbf{x}_k|}\right)^b\right] \\ &= n_c \epsilon_s \left(\frac{N_c}{2}(N_c - 1) + \sum_{i<k}^{N_c} \mathcal{O}(x_{ik}/R)\right) \\ &\quad + n_c \epsilon_h \sum_{i<k}^{N_c} \left(\frac{r_0}{x_{ik}}\right)^b \\ &\approx n_c \epsilon_s \frac{N_c}{2}(N_c - 1) + n_c \epsilon_h N_c \gamma_C \left(\frac{r_0}{\hat{x}}\right)^b, \end{aligned} \quad (5)$$

where x_{ik} is the distance between the ith and kth particle in one cluster, so that $|x_{ik}| < d_c$, where d_c is the diameter of the cluster, which is also smaller than the intercluster distance, $d_c < \bar{x}$. The last approximation in Eq. (5) is obtained by considering $|x_{ik}|/R \ll 1$, and also restricting interactions with the hard-core potential to the first neighbors. Now, the constant γ_C is the number of first neighbors in the intracluster lattice ($\gamma_C = 6$ in the hexagonal case). E_C in Eq. (5) contains a term coming from the soft-core part of the potential and another involving the hard-core one, which takes into account the internal structure of the clusters. Using $N = n_c N_c$ and

$N_c = \bar{x}^2\rho_0/\chi$, we find (neglecting a constant term)

$$E_C = N\left[\epsilon_s \frac{\rho_0}{\chi}\frac{\bar{x}^2}{2} + \epsilon_h \gamma_C \left(\frac{r_0}{\hat{x}}\right)^b\right]. \tag{6}$$

We can see from this expression that the cluster self-energy favors the equilibrium configuration, where clusters are near (because of the term $\propto \bar{x}^2$) but with particles inside them far from each other (because of the term proportional to $1/\hat{x}^b$).

Let us next obtain an expression for the interaction energy among first-neighbors clusters E_I, starting from Eq. (4). The distance between two particles in different clusters can be written as $|\mathbf{x}_{i_a} - \mathbf{x}_{k_b}| = |(\bar{x} + z_{i_a k_b})\hat{\mathbf{z}} + y_{i_a k_b}\hat{\mathbf{y}}|$, where $\bar{x} + z_{i_a k_b}$ is the distance between the particles of two different clusters projected onto the direction of the unit vector $\hat{\mathbf{z}}$ parallel to the line connecting cluster centers; $y_{i_a k_b}$ is the projection of the same distance on the orthogonal axis of unit vector $\hat{\mathbf{y}}$. In this way we have separated the distance between two particles in different clusters as a sum of the distance between the centers of the two clusters $\bar{x}$ and the remaining part $z_{i_a k_b}$, which is smaller than the diameter of cluster d_c. Taking into account the specific shape of the potentials,

$$\begin{aligned} E_I &= n_c \frac{\gamma_I}{2} \sum_{k_b, i_a=1}^{N_c} \left[\epsilon_s e^{-(|(\bar{x}+z_{i_a k_b})\hat{\mathbf{z}} + y_{i_a k_b}\hat{\mathbf{y}}|/R)^\alpha} \right. \\ &\quad \left. + \epsilon_h \left(\frac{r_0}{|(\bar{x} + z_{i_a k_b})\hat{\mathbf{z}} + y_{i_a k_b}\hat{\mathbf{y}}|}\right)^b\right] \\ &\approx n_c \frac{\gamma_I}{2} \sum_{k_b, i_a=1}^{N_c} \epsilon_s e^{-(|(\bar{x}+z_{i_a k_b})\hat{\mathbf{z}} + y_{i_a k_b}\hat{\mathbf{y}}|/R)^\alpha}, \end{aligned} \tag{7}$$

where we have neglected the term $\mathcal{O}[r_0/|(\bar{x} + z_{i_a k_b})\hat{\mathbf{z}} + y_{i_a k_b}\hat{\mathbf{y}}|] \ll 1$, since $\bar{x} \gg r_0$. The role of the hard core is present in this expression through $z_{i_a k_b}$ and $y_{i_a k_b}$ in the exponential, which is not negligible and gives a nontrivial contribution. Note that taking into account the microscopic structure inside a cluster is crucial for the microscale: the appearance of $z_{i_a k_b}$ and $y_{i_a k_b}$ in Eq. (7) gives the only dependence on $\hat{x}$ that can balance the $1/\hat{x}^b$ term appearing in the cluster self-energy Eq. (6). If this dependence on $\hat{x}$ is neglected, it would be impossible to find any equilibrium value $\hat{x}_e$.

To close our problem we need to write the distance $|(\bar{x} + z_{i_a k_b})\hat{\mathbf{z}} + y_{i_a k_b}\hat{\mathbf{y}}|$ in terms of $\hat{x}$ and $\bar{x}$ in order to express E_I in terms of these two distances. One of the possible approximations, which we call a line approximation (LA), consists in neglecting the y coordinate of the particles so that each hexagonal cluster becomes compressed onto a line. Since, as noted above, the direction z joining cluster centers coincides with the hexagonal cluster apothems, the LA considers all particles concentrated on these apothems. See Fig. 4, panel (d), for a drawing of this procedure. By calling n the number of particles located on one external side of a hexagonal cluster, the approximation projects particle positions into one of the $2n-1$ sites, separated by a distance $\hat{x}\sqrt{3}/2$, located in a line along the z direction [see Fig. 4(d)]. Each site now contains more than one particle, with a degeneracy which is maximum in the middle of the cluster and minimum at its extremal points.

n is related to N_c by $N_c = 3n(n-1)+1$. Since $N_c = \bar{x}^2\rho_0/\chi$, we can express n as a function of $\bar{x}$. For large hexagons $n \gg 1$, we have $n \approx \bar{x}(\rho_0/3\chi)^{1/2}$. Using that $n_c = N/N_c = N/\chi\rho_0\bar{x}^2$, we can easily find an approximation for E_I:

$$E_I \approx \epsilon_s N \frac{\chi}{\rho_0}\frac{1}{\bar{x}^2}\gamma_I \sum_{\mu_a,\mu_b=1}^{2n-1} g^{\mu_a} g^{\mu_b} e^{-(|\bar{x}+(\mu_a+\mu_b-2n)\frac{\sqrt{3}}{2}\hat{x}|/R)^\alpha}, \tag{8}$$

where the sum is over all sites, μ_a and μ_b, in the lines that approximate the particle positions in two contiguous clusters. The product $g^{\mu_a} g^{\mu_b}$ gives the degeneracy arising from the number of particles associated to each site in each of the two lines: $g^\nu = n - 1 + \nu$ for $\nu \in [1, n]$ and $g^\nu = 3n - 1 - \nu$ for $\nu \in [n+1, 2n-1]$ [Fig. 4(d)].

Unlike the expression for the cluster self-energy, Eq. (6), E_I favors the configurations for which the mean cluster distance $\bar{x}$ is large but $\hat{x}$ (the intracluster particle distance) is small, as will be seen later.

To better display the dependencies, we normalize both the sum in Eq. (8) (which scales as $\sim n^2$) and the degeneracy g^{μ_a}, introducing $\tilde{g}^{\mu_a} = g^{\mu_a}/n$. Considering the previous relation between n and $\bar{x}$, and combining Eqs. (6) and (8),

$$\begin{aligned} \frac{E(\bar{x},\hat{x})}{N} &= \epsilon_s \frac{\rho_0}{\chi}\frac{\bar{x}^2}{2} + \epsilon_h \gamma_C \left(\frac{r_0}{\hat{x}}\right)^b + \epsilon_s \frac{\rho_0 \bar{x}^2}{9}\frac{\gamma_I}{\chi}\frac{1}{n^2} \\ &\quad \times \sum_{\mu_a,\mu_b=1}^{2n-1} \tilde{g}^{\mu_a}\tilde{g}^{\mu_b} e^{-(|\bar{x}+(\mu_a+\mu_b-2n)\frac{\sqrt{3}}{2}\hat{x}|/R)^\alpha}. \end{aligned} \tag{9}$$

Equation (9) is our main analytical result. It contains three terms which help us to understand the different effects giving rise to the crystal cluster-crystal phase arising at very low temperatures. The first term describes the tendency of the soft potential to favor clusters as close as possible (small $\bar{x}$), simply since in this way, at constant mean density ρ_0, each cluster would be less populated and the internal repulsion will be smaller. This tendency is opposed by the third term, which comes also from the soft potential and contains coupled geometric contributions from both $\bar{x}$ and $\hat{x}$. With respect to the $\bar{x}$ dependence, the third term in Eq. (9) is approximatively $\propto \bar{x}^2 \exp[-(\bar{x}/R)^\alpha]$ if we neglect the weak influence of $\hat{x}$. The interplay between this dependence of the third term and the $\bar{x}^2$ dependence of the first one singles out two values of $\bar{x}$ by energy minimization: $\bar{x}_m = 0$ and $\bar{x}_e > R$. The first one, and in general the values coming from Eq. (9) for $\bar{x} < R$, are not reliable within the approximations used: when $\bar{x} < R$ interactions with clusters beyond nearest neighbors would need to be taken into account, which would raise the energy. Also, the condition of having a cluster lattice without empty clusters implies $\bar{x} \geqslant l \approx L/\sqrt{N}$. Indeed, if $\bar{x} = l$ the clusters have population equal to 1 ($N_c = 1$) and the cluster self-energy is equal to zero; thus exploring $\bar{x}$ below this limit is meaningless. Then, neglecting the behavior for $\bar{x} < R$, the interplay between the first and third terms selects at zero temperature an equilibrium value $\bar{x} > R$ which we call $\bar{x}_e$ [see Figs. 4(a) and 4(c)]. $\bar{x}_e$ is nearly insensitive to the value of $\hat{x}$.

The second term in Eq. (9) arises from the hard-core potential and simply expresses that this short-range repulsion

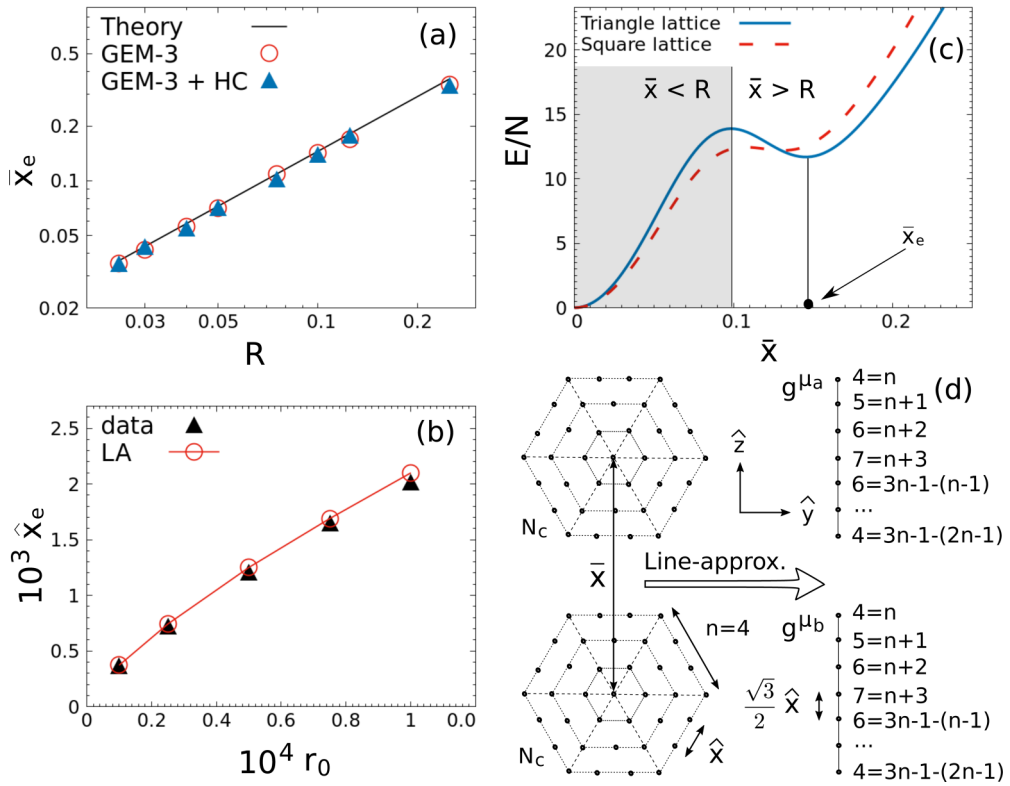

FIG. 4. Left panels: $\hat{x}_e$ and $\bar{x}_e$ vs R [panel (a)] and r_0 [panel (b)], obtained from the simulation of the particle dynamics (symbols) and from minimization of expression (9) for $E(\bar{x}, \hat{x})$ (lines), assuming hexagonal intracluster and intercluster lattices. The theoretical line in panel (a) is indistinguishable from the line $\bar{x}_e \approx 1.45R$ resulting from minimizing Eq. (9) neglecting the hard core. Panel (c): $E(\bar{x}, \hat{x}_e)$ vs $\bar{x}$ at the minimum of the intracluster particle distance $\hat{x}_e$ (with $\gamma_C = 6$) for a square intercluster lattice (red dashed line) and a hexagonal one (blue solid line). The black point stems from $\bar{x}_e$ from the Brownian simulations, which coincides with the lowest energy minimum, which occurs for the hexagonal configuration. As discussed in the text, the dashed region $\bar{x} < R$ and then the additional minimum occurring at $\bar{x} = 0$ should be disregarded since our expressions are not valid there. Panel (d): Graphical illustration of the line approximation (LA), discussed in the text, for a pair of contiguous clusters with $n = 4$. Numbers in the right give the values of the degeneracy factors g^{μ_a} and g^{μ_b}, counting the number of particles projected by the LA onto the same site in the vertical line. Parameters: $D = 10^{-6}$, $r_0/R = 10^{-2}$, $\epsilon_s = \epsilon_h = 1$, $L = 1$, $N = 10^3$, $\alpha = 3$, $b = 6$.

favors large $\hat{x}$. Again, the third term balances this tendency, since larger $\hat{x}$ imply that some particles of different clusters come closer (the particles such that $\mu_a + \mu_b - 2n < 0$), which is unfavorable for the soft-core intercluster repulsion. The balance between the two tendencies determines the zero-temperature equilibrium value of $\hat{x}$, which we call $\hat{x}_e$. Taking into account the $\hat{x}$ dependence in Eq. (8) is crucial to predict a finite $\hat{x}_e$. Indeed, this is the only dependence which can balance the repulsive $1/\hat{x}^b$ term appearing in the cluster self-energy. We also note that if $\epsilon_h = 0$ all particles in a cluster would collapse to its center ($\hat{x} = 0$), which is indeed what happens at zero temperature in the absence of the hard-core potential.

In order to check our approximate expression, in Fig. 4 we plot as functions of R and r_0 the equilibrium intercluster distance $\bar{x}_e$ and the equilibrium interparticle distance inside a cluster $\hat{x}_e$ as obtained from numerical simulations of the Brownian set of particles, showing a good agreement with the theoretical prediction from the minimization of our energy expression. In particular, in the case of the intercluster distance [Fig. 4(a)] we compare the prediction with two different simulation settings, with and without the hard-core potential (purely soft-core potential). As expected, the smaller scale does not influence much the intercluster distance $\bar{x}_e$, which is quite constant with respect to r_0, for $r_0 \ll R$. This confirms, in agreement with [11], that the microscopic details of the clusters are macroscopically less relevant. The relevance of the small scale appears in determining the intracluster distance $\hat{x}_e$ [Fig. 4(b)], which depends strongly on r_0, and so on the average size of the clusters (which is roughly $\hat{x}_e\sqrt{N_c}$).

Figure 4(c) plots $E(\bar{x}, \hat{x} = \hat{x}_e)$ as a function of the intercluster distance $\bar{x}$ for parameters χ and γ_I corresponding to two different cluster lattices (hexagonal and square). It is seen that the hexagonal minimum is lower [remember than the minimum at $\bar{x} = 0$ and the whole region $\bar{x} < R$ should be disregarded as Eq. (9) is not valid there], implying that the hexagonal cluster crystal is the most stable. Similar results appear in [12] for the hard-core solft-shoulder potentials in the context of the lattice description.

IV. FINITE-TEMPERATURE CORRECTIONS

The theoretical results of the previous section are approximately valid only in the limit of vanishing temperature. At finite temperature, energy minimization should be replaced by free-energy minimization, which requires one to take into

account the role of entropy S. Approaches in this line for the lattice shoulder potential can be found in [11,12]. In this section, we estimate the free energy and use it to characterize temperature effects on the cluster structure.

In principle, we can distinguish between different entropic sources: the intercluster entropy S_I, which takes into account the defects of the cluster-crystal lattice, and the internal entropy of the clusters S_C. In general, $S_I \ll S_C$, if $N_C \gg 1$ since, roughly, $S_I \propto n_c = N/N_c$ and $S_C \propto N$. For this reason, we focus on the calculation of $S_C \approx S$, which strongly depends on the intracluster regime we are considering. Below, we compute it in the crystal cluster-crystal and in the fluid (gaslike) cluster-crystal phases, where we developed reasonable approximations for the probability distribution of the particle positions. In an intermediate liquid cluster-crystal regime, the situation is different, since all the intracluster particles have positions correlated in a nontrivial way, as usual in the framework of liquid theory. We point out that in the fluid cluster-crystal regime, S_C plays a fundamental role in determining the average size of the cluster, in agreement with [10] for purely soft-core potentials.

A. Very low temperature: Crystal cluster-crystal phase

We consider first the situation of very low temperature in which the cluster crystal with crystalline interior remains and neglect any temperature influence in the positions of the cluster centers (which then remain in a hexagonal lattice of intercluster distance $\bar{x}_e$). In the same way, we assume that particles inside each cluster remain close to the positions in the hexagonal lattice of distance $\hat{x}_e$, which characterizes the zero-temperature equilibrium state. This implies neglecting any thermal dilation effect which could affect $\bar{x}_e$ or $\hat{x}_e$. The only temperature effect we estimate now is the possible vibration of each particle around its equilibrium position, characterized by a vibration width σ_h. To this end, we concentrate on the vibrational entropy S_v, neglecting any *translational* entropy associated with the displacement of the equilibrium particle positions, which will eventually favor the formation of defects.

We make a further mean-field-like approximation in order to evaluate S_v: interactions among particles are already taken into account in determining the lattice constants $\bar{x}_e$ and $\hat{x}_e$, and we neglect any further effect in producing particle-position correlations. More specifically, we assume the N-particle probability of positions to factorize: $P_N(\mathbf{x}_1,\ldots,\mathbf{x}_N) = \prod_{a=1}^{n_c}\prod_{i_a=1}^{N_c} p(\mathbf{x}_{i_a} - \mathbf{u}_{i_a})$, where the first product runs over the n_c clusters and the second over $\{\mathbf{u}_{i_a}\}$, the (zero-temperature) equilibrium positions of the particles. $p(\mathbf{x})$ gives the probability distribution of the position fluctuations of each particle around its equilibrium. We consider the same $p(\mathbf{x})$ for each particle, independently of its position in the cluster. Then, the entropy associated to P_N becomes a sum of terms, one for each particle:

$$S_v = n_c N_c S_1, \quad S_1 = -k_B \int d\mathbf{x}\, p(\mathbf{x}) \log(p(\mathbf{x})/\rho_0). \tag{10}$$

Our strong-localization assumption implies that no combinatorial factor coming from indistinguishability needs to be used. Our final assumption is that at very low temperatures $p(\mathbf{x})$ is a narrow two-dimensional Gaussian of width σ_h [20], so that

$$\begin{aligned} S_v &= -k_B n_c N_c \int d\mathbf{x} \frac{e^{-\mathbf{x}^2/2\sigma_h^2}}{2\pi\sigma_h^2} \log\left(\frac{e^{-\mathbf{x}^2/2\sigma_h^2}}{2\pi\sigma_h^2\rho_0}\right) \\ &= k_B n_c N_c \left[1 + \log(2\pi) + \log\left(\sigma_h^2\rho_0\right)\right]. \end{aligned} \tag{11}$$

We have used that for a two-dimensional isotropic Gaussian variable, $\langle \mathbf{x}^2\rangle = \langle x^2\rangle + \langle y^2\rangle = 2\sigma_h^2$. The width σ_h is the only remaining parameter and will be determined from the minimization of the free energy. To be consistent with the approximations used, the resulting width should satisfy $\sigma_h \ll \hat{x}$.

Next, we evaluate the average energy of the system, separated in intracluster and intercluster interactions:

$$\begin{aligned} \langle E\rangle &= \langle E_C\rangle + \langle E_I\rangle \\ &= \sum_{a=1}^{n_c}\sum_{i_a<j_a}^{N_c} \int d\{\mathbf{x}\}_N P_N(\mathbf{x}_1,\ldots,\mathbf{x}_N) V\left(\mathbf{x}_{i_a} - \mathbf{x}_{j_a}\right) \\ &\quad + \sum_{a=1}^{n_c}\sum_{a<b}^{n_c}\sum_{i_a,j_b}^{N_c} \int d\{\mathbf{x}\}_N P_N(\mathbf{x}_1,\ldots,\mathbf{x}_N) V\left(\mathbf{x}_{i_a} - \mathbf{x}_{j_b}\right). \end{aligned} \tag{12}$$

Under the same approximate mean-field framework as for the entropy, we split P_N into a product of single-particle (Gaussian) probabilities. For the intracluster part we arrive to

$$\begin{aligned} \langle E_C\rangle &\approx n_c \frac{N_c}{2} \int d\mathbf{x}_1 d\mathbf{x}_2 \frac{e^{-\mathbf{x}_1^2/2\sigma_h^2}}{2\pi\sigma_h^2} \frac{e^{-\mathbf{x}_2^2/2\sigma_h^2}}{2\pi\sigma_h^2} \\ &\quad \times \sum_{j\neq 0} V(\mathbf{x}_1 - \mathbf{a}_j - \mathbf{x}_2) \\ &= n_c \frac{N_c}{2} \int d\mathbf{z} \frac{e^{-\mathbf{z}^2/4\sigma_h^2}}{4\pi\sigma_h^2} \sum_{j\neq 0} V(\mathbf{z} - \mathbf{a}_j)\,. \end{aligned} \tag{13}$$

The sum is over all position vectors $\{\mathbf{a}_j\}$ of the equilibrium positions of the particles inside a cluster (except the one at $\mathbf{a}_0 = \mathbf{0}$, where we have arbitrarily located the equilibrium position of the first particle), which form a hexagonal lattice. The last equality is obtained after changing variables to the average, $\mathbf{u} = (\mathbf{x}_1 + \mathbf{x}_2)/2$, and relative, $\mathbf{z} = \mathbf{x}_1 - \mathbf{x}_2$, coordinates and integrating over $\mathbf{u}$.

The interaction potential is made of the hard-core and the soft-core parts, $V(\mathbf{x}) = V_h(|\mathbf{x}|) + V_s(|\mathbf{x}|)$. Since the Gaussian restricts the integration to a region of size σ_h around the origin and we are assuming $R \gg \hat{x}_e \gg \sigma_h$, the soft-core potential is effectively constant inside the integral, $V_s(|\mathbf{x}|) = \epsilon_s[1 + \mathcal{O}(\sigma_h/R)^2]$ and then $\sum_{j\neq 0} V_s(|\mathbf{v} - \mathbf{a}_j|) \approx (N_c - 1)\epsilon_s$. For the hard-core potential we approximate the interaction sum by the contribution from the nearest neighbors of the particle at the origin, which are at the corners of a hexagon $(\mathbf{a}_1,\ldots,\mathbf{a}_6$, with $|\mathbf{a}_i| = \hat{x}_e)$ (see upper-right panel of Fig. 2). Expanding the interaction sum in the vicinity of $\mathbf{z} = \mathbf{0}$,

$$\begin{aligned} &\sum_{i=1}^{6} V_h(|\mathbf{z} - \mathbf{a}_i|) \\ &\quad \approx 6V_h(\hat{x}_e) + \frac{3}{2}\left(V_h(\hat{x}_e)'' + \frac{V_h(\hat{x}_e)'}{\hat{x}_e}\right)\mathbf{z}^2 + \cdots. \end{aligned} \tag{14}$$

The terms neglected are of order z_x^4, z_y^4, and $z_x^2 z_y^2$, and thus will give corrections smaller than $(\sigma_h/\hat{x}_e)^4$. By introducing Eq. (13) and performing the integration,

$$\langle E_C\rangle \approx n_c \frac{N_c}{2}\Big[(N_c-1)\epsilon_s + 6V_h(\hat{x}_e) + 6\Big(V_h(\hat{x}_e)'' + \frac{V_h(\hat{x}_e)'}{\hat{x}_e}\Big)\sigma_h^2\Big]. \quad (15)$$

Considering now the intracluster part of the mean energy, we again factorize the N-particle probability. In the previous section, the contribution of the particle positions inside the cluster to E_I was needed to properly determine the interparticle distance $\hat{x}$. But here, once we take this as fixed, we estimate the temperature corrections to $\langle E_I\rangle$ by assuming that all particle equilibrium positions are at the center of the cluster they belong. Under this approximation,

$$\langle E_I\rangle \approx n_c \frac{N_c^2}{2}\int d\mathbf{x}_1 d\mathbf{x}_2 \frac{e^{-\mathbf{x}_1^2/2\sigma_h^2}}{2\pi\sigma_h^2}\frac{e^{-\mathbf{x}_2^2/2\sigma_h^2}}{2\pi\sigma_h^2} \times \sum_{b\neq 0} V(\mathbf{x}_1-\mathbf{b}_b-\mathbf{x}_2). \quad (16)$$

The sum is now over all position vectors $\{\mathbf{b}_b\}$ of the cluster centers (except the one we arbitrarily locate at $\mathbf{b}_0=\mathbf{0}$), which forms again a hexagonal lattice.

Since $r_0 \ll \bar{x}_e = \min_{b\neq 0}\{|\mathbf{b}_b|\}$, the contribution of the hard-core potential to $\langle E_I\rangle$ is negligible. As before, except for corrections which are $\mathcal{O}(\sigma_h/R)^2$, the soft-core potential in each term of the sum can be considered constant inside the integral. Restricting the sum to the six clusters surrounding (at distance $\hat{x}_e$) the one at the origin, we find

$$\langle E_I\rangle \approx n_c \frac{N_c^2}{2} 6V_s(\bar{x}_e). \quad (17)$$

We can now write the full expression for the free energy:

$$\frac{F}{n_c N_c} = \frac{\langle E\rangle - TS}{n_c N_c} \approx \frac{E_0}{n_c N_c} - D[1+\log(2\pi)] + 3\Big(V_h(\hat{x}_e)'' + \frac{V_h(\hat{x}_e)'}{\hat{x}_e}\Big)\sigma_h^2 - D\log(\sigma_h^2\rho_0), \quad (18)$$

where we have used $D=k_BT$, and we have collected all terms of the mean energy which are independent of σ_h into the constant E_0. By minimizing with respect to σ_h and taking the explicit forms for V_s and V_h we find

$$\sigma_h^2 = \frac{D}{3(V_h(\hat{x}_e)'' + V_h(\hat{x}_e)'/\hat{x}_e)} = \frac{D\hat{x}_e^2(\hat{x}_e/r_0)^b}{3b^2\epsilon_h}, \quad (19)$$

which is the expression characterizing the influence of temperature on the fluctuations of each particle position around its equilibrium location. Note that this is precisely the expression for the standard deviation of the Gaussian probability which describes the motion of a Brownian particle in the harmonic approximation, close to the origin, due to the combined potential of six particles at hexagonal positions surrounding the origin at distance $\hat{x}_e$. The consistency condition $\sigma_h \ll \hat{x}_e$ implies that Eq. (19) is only valid at small temperatures such that $D \ll D_h = 3b^2\epsilon_h(r_0/\hat{x}_e)^b$. One may think that D_h gives a rough estimation of the transition temperature above which the crystalline structure inside the clusters is lost (probably into a liquidlike phase), but we think it is at best a rough upper bound because of the many approximations involved. In a liquidlike phase particles do not fluctuate around any equilibrium points. Moreover, the dynamics is correlated, meaning that the main hypothesis of our calculation is not satisfied. By minimizing Eq. (18) also with respect to the intra- and intercluster distances, we can obtain entropic corrections to them. These corrections are $\mathcal{O}(D)$ and therefore very small in this phase.

B. Fluid cluster-crystal phase

Numerical simulations indicate that there is a range of temperatures in which clusters remain but particles inside them do not display a crystal structure but a fluidlike behavior. This implies that thermal motion inside the cluster has exceeded the capacity of the hard-core potential to keep the particles in place, as it would occur if $D \gtrsim D_h$. Because of this, and since we know that clusters appear because of the nature of the soft-core repulsion (forming a large hexagonal lattice with lattice vectors $\{\mathbf{b}_b\}$), we describe this fluid cluster-crystal state by completely neglecting the hard-core potential, i.e., $V(\mathbf{x}) \approx V_s(|\mathbf{x}|)$. In this gaslike situation, we now estimate how the cluster width σ_s depends on temperature.

In the same mean-field approach as before, we consider that the many-body probability P_N factorizes into single-particle Gaussians—but this time of width σ_s—characterizing cluster size, since each particle can explore the whole cluster in the fluid state. A consistency condition is that $\sigma_s \ll \bar{x}_e$ for the crystal-cluster structure to remain, despite the finite size of the clusters. In fact, we should also have $\hat{x}_e\sqrt{N_c} \ll \sigma_s$, since the first term is an estimation of the size of a cluster of N_c particles in the low-temperature regime, within which it retains a crystal structure. Similarly to the previous low-temperature case [see Eq. (11)], the vibrational entropy will be

$$S_v = k_B n_c N_c\big[1+\log(2\pi)+\log\big(\sigma_s^2\rho_0\big)\big]. \quad (20)$$

For the mean energy, we distinguish again the cluster self-energy $\langle E_C\rangle$ and the intercluster contribution $\langle E_I\rangle$. For this last quantity, we introduce the probability factorization into Eq. (12) to obtain [cf. Eq. (16)]

$$\langle E_I\rangle \approx \frac{n_c N_c^2}{2}\int d\mathbf{x}_1 d\mathbf{x}_2 \frac{e^{-\mathbf{x}_1^2/2\sigma_s^2}}{2\pi\sigma_s^2}\frac{e^{-\mathbf{x}_2^2/2\sigma_s^2}}{2\pi\sigma_s^2} \times \sum_{b=1}^{6} V_s(|\mathbf{x}_1-\mathbf{b}_b-\mathbf{x}_2|) = \frac{n_c N_c^2}{2}\int d\mathbf{z}\frac{e^{-\mathbf{z}^2/4\sigma_s^2}}{4\pi\sigma_s^2}\sum_{b=1}^{6} V_s(|\mathbf{z}-\mathbf{b}_b|). \quad (21)$$

We have approximated all equilibrium particle positions as located at the center of the cluster they belong, and interactions have been restricted to the six clusters (with $|\mathbf{b}_b|=\bar{x}_e$) neighboring the first one, which we have arbitrarily located at

the origin. The last equality is obtained after transforming to relative and center-of-mass coordinates and integrating over the last one. Using the expansion [cf. Eq. (14)]

$$\sum_{b=1}^{6} V_s(|\mathbf{z}-\mathbf{b}_b|) \approx 6V_s(\bar{x}_e) + \frac{3}{2}\left(V_s(\bar{x}_e)'' + \frac{V_s(\bar{x}_e)'}{\bar{x}_e}\right)\mathbf{z}^2 + \cdots, \quad (22)$$

we obtain

$$\langle E_I\rangle \approx 3n_c N_c^2\left[V_s(\bar{x}_e) + \left(V_s(\bar{x}_e)'' + \frac{V_s(\bar{x}_e)'}{\bar{x}_e}\right)\sigma_s^2\right]. \quad (23)$$

The intracluster self-energy reads

$$\langle E_C\rangle \approx n_c\frac{N_c}{2}\int d\mathbf{x}_1 d\mathbf{x}_j \frac{e^{-\mathbf{x}_1^2/2\sigma_s^2}}{2\pi\sigma_s^2}\frac{e^{-\mathbf{x}_2^2/2\sigma_s^2}}{2\pi\sigma_s^2}\sum_{j\neq 1}^{N_c} V_s(|\mathbf{x}_1-\mathbf{x}_j|) = n_c\frac{N_c(N_c-1)}{2}\int d\mathbf{z}\frac{e^{-\mathbf{z}^2/4\sigma_s^2}}{4\pi\sigma_s^2}V_s(|\mathbf{z}|). \quad (24)$$

For the GEM-α potential, $V_s(|\mathbf{z}|) = \epsilon_s[1+\mathcal{O}(|\mathbf{z}/R|^\alpha)]$, being the last term negligible if $\alpha > 2$, compared to the terms already considered in Eq. (22). This is precisely the reason why cluster crystals form in a GEM-α potential with $\alpha > 2$: the particle repulsion inside the cluster is negligible compared with the repulsion from the neighboring clusters [10]. Thus, neglecting terms smaller than $\mathcal{O}(|\sigma_s/R|^2)$,

$$\langle E_C\rangle \approx n_c\frac{N_c(N_c-1)}{2}\epsilon_s. \quad (25)$$

The complete expression for the free energy in this fluid or gas cluster regime is

$$\frac{F}{n_c N_c} = \frac{\langle E\rangle - TS}{n_c N_c} \approx \frac{\tilde{E}_0}{n_c N_c} - D[1+\log(2\pi)] + 3N_c\left(V_s(\bar{x}_e)'' + \frac{V_s(\bar{x}_e)'}{\bar{x}_e}\right)\sigma_s^2 - D\log\left(\sigma_s^2\rho_0\right). \quad (26)$$

All terms of the mean energy which are independent of σ_s have been included in $\tilde{E}_0$. Minimizing with respect to σ_s and taking our explicit expression for V_s gives

$$\sigma_s^2 = \frac{D}{3N_c[V_s(\bar{x}_e)'' + V_s(\bar{x}_e)'/\bar{x}_e]} = \frac{D\bar{x}_e^2 e^{(\bar{x}_e/R)^\alpha}(R/\bar{x}_e)^\alpha}{3\alpha^2\epsilon_s N_c[(\bar{x}_e/R)^\alpha - 1]}. \quad (27)$$

As in Eq. (19), this is the width of the Gaussian probability distribution for a Brownian particle moving in the combined potential of six clusters located on the corners of a hexagon at distance $\bar{x}_e$ from the origin, each providing a repulsion given by the potential $N_c V_s$, and under the harmonic approximation close to the origin. It also coincides, after noting that the number of particles in each cluster of a hexagonal cluster crystal is $N_c = \rho_0\sqrt{3}\bar{x}_e^2/2$, with the cluster width derived from approximations to the Dean-Kawasaki equation in a GEM-α potential [10]. We recall that expression (27) is expected to be valid only in the intermediate-temperature range such that $\hat{x}_e\sqrt{N_c} \ll \sigma_s \ll \bar{x}_e$. Violation of the last inequality, i.e., $\sigma_s \approx \bar{x}_e$, gives a rough upper limit to the melting temperature of the cluster crystal. The results in [10] indicate that indeed this estimation overestimates the cluster-crystal melting temperature (for the system in which only the interaction V_s is present), although the qualitative parameter dependence is correct. As a final remark, minimizing Eq. (26) with respect to the intercluster distance would allow us to estimate the temperature corrections in determining $\bar{x}_e$. These corrections are all $\mathcal{O}(D)$.

V. SUMMARY AND DISCUSSION

We have studied the influence of a hard-core potential on the cluster-crystal phase of a system of particles interacting through a GEM-α repulsive potential. Performing off-lattice numerical simulations of the interacting Brownian particles, we have identified the different ordering types that particles inside the clusters exhibit. Temperature drives a transition from a crystal cluster-crystal scenario (where particles within clusters are periodically ordered) to a fluid or gas cluster-crystal form. In the small temperature limit, an energy expression has been obtained which helps to understand the balances between the different forces leading to the existence of the cluster-crystal phase. In addition, the finite-temperature value of the cluster width has been obtained for the fluid cluster-crystal state, and also for the fluctuation amplitude of the particles around their equilibrium positions in the crystal cluster-crystal state. They provide rough upper limits to the temperatures at which transitions would take place.

The methodology employed is rather general, and other types of potentials leading to cluster crystals could be considered. See, for instance, the soft potential in [21,22] in the context of bosonic interactions. Furthermore, we expect our approach to be of use to describe biological aggregations in which the individuals have a finite size and interact through forces acting attractively or repulsively at different scales or through competing or mutualistic dynamics [23]. The generalization of our study to nonequilibrium systems of particles with finite size and interacting through repulsive forces is of much interest in the context of active matter and will be considered in the future, extending approaches such as those in Ref. [24].

ACKNOWLEDGMENTS

We acknowledge financial support from the Spanish Grants LAOP CTM2015-66407-P (AEI/FEDER, EU) and ESOTECOS FIS2015-63628-C2-1-R (AEI/FEDER, EU). We acknowledge fruitful discussions and continuous support from Profs. Umberto Marini Bettolo Marconi and Angelo Vulpiani.

[1] C. N. Likos, F. Sciortino, and E. Zaccarelli, *Soft Matter Self-Assembly* (IOS Press, Amsterdam, 2016).
[2] W. Klein, H. Gould, R. A. Ramos, I. Clejan, and A. I. Mel'cuk, Phys. A (Amsterdam, Neth.) **205**, 738 (1994).
[3] C. N. Likos, A. Lang, M. Watzlawek, and H. Löwen, Phys. Rev. E **63**, 031206 (2001).
[4] B. M. Mladek, D. Gottwald, G. Kahl, M. Neumann, and C. N. Likos, Phys. Rev. Lett. **96**, 045701 (2006).
[5] C. N. Likos, B. M. Mladek, D. Gottwald, and G. Kahl, J. Chem. Phys. **126**, 224502 (2007).
[6] B. M. Mladek, G. Kahl, and C. N. Likos, Phys. Rev. Lett. **100**, 028301 (2008).
[7] D. Coslovich and A. Ikeda, Soft Matter **9**, 6786 (2013).
[8] C. N. Likos, Phys. Rep. **348**, 267 (2001).
[9] C. N. Likos, H. Löwen, M. Watzlawek, B. Abbas, O. Jucknischke, J. Allgaier, and D. Richter, Phys. Rev. Lett. **80**, 4450 (1998).
[10] J. B. Delfau, H. Ollivier, C. López, B. Blasius, E. Hernández-García, Phys. Rev. E **94**, 042120 (2016).
[11] M. A. Glaser, G. M. Grason, R. D. Kamien, A. Košmrlj, C. D. Santangelo, and P. Ziherl, Europhys. Lett. **78**, 46004 (2007).
[12] H. Shin, G. M. Grason, and C. D. Santangelo, Soft Matter **5**, 3629 (2009).
[13] P. Ziherl and R. D. Kamien, J. Phys. Chem. B **115**, 7200 (2011).
[14] F. Sciortino, S. Mossa, E. Zaccarelli, and P. Tartaglia, Phys. Rev. Lett. **93**, 055701 (2004).
[15] S. Mossa, F. Sciortino, P. Tartaglia, and E. Zaccarelli, Langmuir **20**, 10756 (2004).
[16] J. C. F. Toledano, F. Sciortino, and E. Zaccarelli, Soft Matter **5**, 2390 (2009).
[17] D. E. Dudalov, E. N. Tsiok, Y. D. Fomin, and V. N. Ryzhov, J. Chem. Phys. **141**, 18C522 (2014).
[18] B. M. Mladek, P. Charbonneau, C. N. Likos, D. Frenkel, and G. Kahl, J. Phys.: Condens. Matter **20**, 494245 (2008).
[19] C. N. Likos, B. M. Mladek, A. J. Moreno, D. Gottwald, and G. Kahl, Comput. Phys. Commun. **179**, 71 (2008).
[20] P. Tarazona, Phys. Rev. A **31**, 2672 (1985).
[21] F. Cinti, M. Boninsegni, and T. Pohl, New J. Phys. **16**, 033038 (2014).
[22] R. Díaz-Méndez, F. Mezzacapo, F. Cinti, W. Lechner, and G. Pupillo, Phys. Rev. E **92**, 052307 (2015).
[23] N. Khalil, C. López, and E. Hernández-García, J. Stat. Mech. (2017) 063505.
[24] J.-B. Delfau, C. L. López, and E. Hernández-García, New J. Phys. **19**, 095001 (2017).